

***In-situ* characterization of femtosecond laser-induced crystallization in borosilicate glass using time-resolved surface third-harmonic generation**

Weimin Liu, Liang Wang, Fangyuan Han, and Chong Fang^{a)}

Department of Chemistry, Oregon State University, Corvallis, Oregon 97331, USA

(Received 25 September 2013; accepted 31 October 2013; published online 14 November 2013)

Coherent phonon dynamics in condensed-phase medium are responsible for important material properties including thermal and electrical conductivities. We report a structural dynamics technique, time-resolved surface third-harmonic generation (TRSTHG) spectroscopy, to capture transient phonon propagation near the surface of polycrystalline CaF₂ and amorphous borosilicate (BK7) glass. Our approach time-resolves the background-free, high-sensitivity third harmonic generation (THG) signal in between the two crossing near-IR pulses. Pronounced intensity quantum beats reveal the impulsively excited low-frequency Raman mode evolution on the femtosecond to picosecond timescale. After amplified laser irradiation, danburite-crystal-like structure units form at the glass surface. This versatile TRSTHG setup paves the way to mechanistically study and design advanced thermoelectrics and photovoltaics. © 2013 AIP Publishing LLC. [<http://dx.doi.org/10.1063/1.4831655>]

Light-induced crystallization in amorphous semiconductors, glass, thin films, organic solutions, and biological molecules has been an intriguing topic in the field of applied physics, physical chemistry, optoelectronics, as well as crystal science and engineering.^{1–4} Understanding material properties during and after crystallization is thus of fundamental and technological interest, and a sensitive probe for microscopic processes that determine macroscopic functions is the molecular vibration. Raman spectroscopy was used to study the vibrational response of amorphous materials such as vitreous SiO₂, where the width of vibrational modes directly reflects the structure disorder.⁵ Time-resolved vibrational coherence spectrum based on impulsive stimulated Raman scattering (ISRS) has been demonstrated.^{6,7} Femtosecond (fs) laser pulse induced coherent lattice vibrational dynamics were studied in semiconductors and metals through several nonlinear optical techniques including second harmonic generation (SHG) and sum frequency generation (SFG),^{8–10} and, more recently, third harmonic generation (THG).^{11,12} These nonlinear optical techniques to explore coupling between electrons and nuclei at surfaces typically use the MHz oscillator output pulses in a pump-probe setup, measuring the reflectivity or transmission changes of the probe at the sample spot upon interaction with the pump pulse.

In this Letter, we report the development of a distinct time-resolved surface third-harmonic generation (TRSTHG) spectroscopy, and the *in-situ* characterization of the fs laser-induced crystallization on the thin borosilicate (BK7) glass surface through coherently excited phonons at the vibrational frequency range of ca. 10–500 cm⁻¹. The acronym TRSTHG emphasizes the ultraviolet (UV) nature of our detected signal from two incident fundamental pulses (FPs) in the near IR (i.e., 800 nm), and the surface-enhancing characteristics of these THG signals generated in between the two FPs. Coherent phonons (CPs) are launched by the

amplified fs pulses that provide broad spectral bandwidth, and the dominant driving force is ISRS that enables us to investigate the generation and relaxation of vibrational coherences. The TRSTHG processes stem from the cubic nonlinear electric susceptibility $\chi^{(3)}$ of the medium that can be expressed as a time-dependent quantity involving the equilibrium value and an atomic position-dependent term,^{13,14} i.e., $\chi^{(3)}(t) = \chi_0^{(3)} + (\partial\chi^{(3)}/\partial Q) \cdot Q(t)$, where $(\partial\chi^{(3)}/\partial Q)$ represents the Raman nonlinearity and $Q(t)$ describes the lattice vibrations in a typical crystal structure, and higher-order insignificant terms are omitted. Upon impulsive generation of CPs in the medium by the fs pulse, the THG signal that originates from the third-order nonlinear optical response will be temporally modulated due to the time dependence of $\chi^{(3)}$ in reference to varying atomic positions on the fs to picosecond (ps) timescale.¹³ Therefore, even without resonance enhancement, the Raman-induced CPs can superimpose a damped oscillatory component on the nonoscillatory decaying component following the ultrafast electronic response around the time zero for excitation.^{15,16}

The prototype experimental setup has been recently reported by us.¹² In brief, the THG signals are generated using a fs Ti:sapphire regenerative amplifier (Legend Elite-USP, Coherent) laser system, which provides 1 kHz, 35 fs pulse train centered at 800 nm. A portion of the FP is separated by a beam-splitter (50R/50T) to ~50 μ J/pulse per arm with the same *p*-polarization, attenuated by an iris and a variable neutral density filter. One of the FP arms (FP₁ in Fig. 1) is fixed to pulse energy of ~6 μ J, while the other arm (FP₂) is tuned within ca. 6–35 μ J/pulse for the power-dependent laser crystallization experiment on glass. The two FPs are tightly focused onto the thin sample using an *f* = 10 cm Ag-coated spherical concave mirror, with beam diameters of ~0.2 mm at the foci and a crossing angle of ~6°. The maximal peak power density of ~3.2 × 10¹² W/cm² is still below the glass damage threshold upon fs pulse irradiation.¹⁸ For time-resolved measurement, FP₁ passes through a high-resolution motor-controlled delay stage (07EAS504,

^{a)} Author to whom correspondence should be addressed. Electronic mail: Chong.Fang@oregonstate.edu

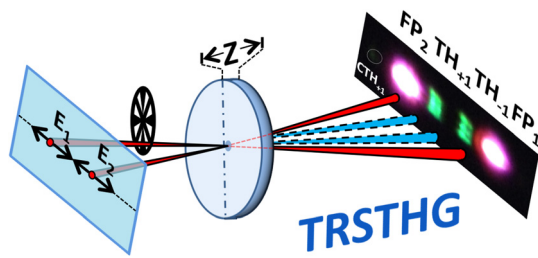


FIG. 1. Delineation of the TRSTHG setup. Transient phonon dynamics can be retrieved by temporally delaying the two incident near-IR fundamental pulses and detecting the UV signals generated in between them. To reduce scattering interference and improve THG signal strength, we measure TH_{+1} that is farther away from the beam being chopped (FP_1). The weak CTH_{+1} signal that arises from cascaded four-wave mixing is circled near the FP_2 beam.

CVI Melles Griot) and is chopped at 500 Hz with a phase-locked optical chopper (3501, Newport). In order to minimize the FP-THG¹² scattering into the detector and to increase the CP generation efficiency, we detect the THG signal closer to the unchopped FP_2 beam [see Fig. 1]. The sideband signal TH_{+1} is focused using an $f=10$ cm fused silica lens, and its UV portion is filtered through a UV band-pass filter (FGUV11, Thorlabs) and measured by a Si biased photodiode detector. The time-dependent signal intensity is then collected via a lock-in amplifier and a computer. All experiments are carried out at the room temperature of 22 °C.

When a laser is tightly focused on a medium, THG processes are weak inside the bulk due to Gouy phase shift; however, this effect is dramatically suppressed at the interface and a much enhanced THG signal is generated.^{11,19} We previously demonstrated that upon tightly focusing two intense near-IR FPs onto a thin glass slide, a series of spatially separated UV sidebands emerge from the glass-air interface due to different third-order nonlinear phase-matching conditions.¹² The most pronounced UV signals $TH_{\pm 1}$ at 267 nm are generated through the interaction of the two crossing FPs, e.g., $\omega_{TH+1} = 2\omega_{FP2} + \omega_{FP1}$ [Fig. 1]. By precisely changing the time delay between the two FPs, we observed oscillatory THG signals in amorphous fused silica. In this work, we first study the vibrational dynamics in a 1-mm-thick calcium fluoride (CaF_2) polycrystalline plate (WFD-U15, Harrick Scientific Products) by measuring the TH_{+1} signal intensity with delay time step of 6.7 fs (FP_1 is preceding), and both FPs at $\sim 6 \mu J/pulse$. The below-band-gap excitation by the near-IR FPs initiates a coherent vibrational-motion-induced macroscopic polarization in the focal volume, wherein the crossing FPs produce light at the distinct THG direction. The highly reproducible oscillation in the THG intensity temporal evolution [Fig. 2] results from coherent scattering due to polarization components at the vibrational mode frequencies. The fast Fourier transform (FFT) spectrum is shown in the inset of Fig. 2, which well matches the standard Raman spectrum of CaF_2 . Several pronounced low-frequency Raman modes are attained because the FP has a ~ 32 nm bandwidth that supports coherent mode excitation up to ~ 500 cm^{-1} . In addition to literature CaF_2 Raman modes²⁰ at ~ 322 , 265, 250, 220, and 157 cm^{-1} , three other modes are clearly observed below 150 cm^{-1} .

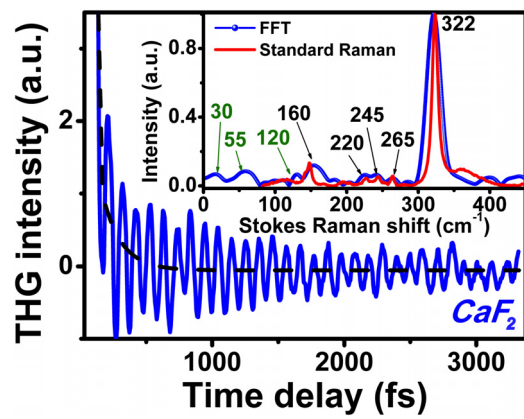


FIG. 2. Transient TRSTHG signal of polycrystalline CaF_2 up to 3.4 ps. The black dashed line shows the exponential fit of the non-oscillatory component. The inset exhibits the low-frequency modes of CaF_2 from FFT (with Blackman window function) of the TH_{+1} intensity temporal oscillatory component (blue), in comparison with the standard Raman spectrum (red).

To unravel the free induction decay of each detected vibrational component, we use continuous Morlet wavelet basis²¹ to perform time-frequency domain analysis. As shown in the two-dimensional contour plot in Fig. 3, the strongest 322 cm^{-1} mode shows a dephasing time of ~ 750 fs measured by the single-exponential fitting. Three acoustic CP modes at ~ 120 , 55, and 30 cm^{-1} reveal different decay time of ca. 400 fs, 800 fs, and 1.6 ps, respectively. These terahertz (THz) modes can be attributed to boson peaks that are commonly observed in amorphous solids, supercooled liquids, and crystals,^{22–24} which in our experiment is a strong indication of polycrystal defects or long-range lattice disorder in polycrystalline CaF_2 under investigation.^{22,23}

The observation of CP dynamics on the surface of CaF_2 demonstrates the potential of our background-free, non-destructive, time-domain technique to study the low-frequency

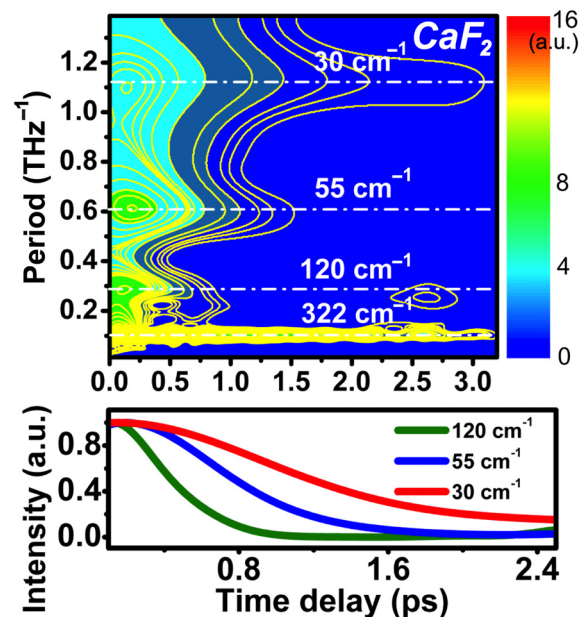


FIG. 3. Morlet wavelet-transformed time-frequency contour plot of the TH_{+1} quantum beats in CaF_2 up to 3.2 ps. Bottom panel manifests different dephasing dynamics for the underlying CP modes, which is indicative of varied structural origins for these low-frequency vibrational peaks. The vertical axis is presented as the normalized intensity of the three modes.

Raman modes (i.e., below $\sim 500\text{ cm}^{-1}$) with high sensitivity. For potential optoelectronic applications, we target the *in-situ* characterization of laser-irradiating reconstruction in BK7 glass. When a fs laser is tightly focused onto a transparent amorphous material, the transient accumulated heat intensity in the focal spot area can become high enough to induce densification of glass through multiphoton absorption and ionization processes, which directly lead to structural changes or crystallization in the material.^{25,26} Such crystallization processes in glass can be used for data storage and direct writing of optical waveguide and optical grating.^{27,28} To avoid nearby UV scattering and increase THG signal-to-noise ratio in glass, the intense unchopped FP₂, besides generating the UV signal via interaction with FP₁, acts as an actinic excitation pulse with sufficient peak power to melt and reform the amorphous phase of glass into the crystalline phase. Notably, the observed TH₊₁ signal can only be generated at the back surface of the glass-air interface¹² because glass is transparent at the FP wavelength region but strongly absorbs in the UV range.

Transient TH₊₁ signal evolution in a 0.15-mm-thick amorphous BK7 glass plate (cover glass, Thermo Scientific) is plotted in Fig. 4(a) as the FP₂ pulse energy is increased from 6 to 35 μJ . We move the sample after laser irradiation and data collection on the same spot for several minutes, to ensure that each time-resolved trace is measured on a pristine area of the glass plate under the specified irradiation power. With FP₂ at 6 $\mu\text{J}/\text{pulse}$, TH₊₁ shows a Gaussian profile

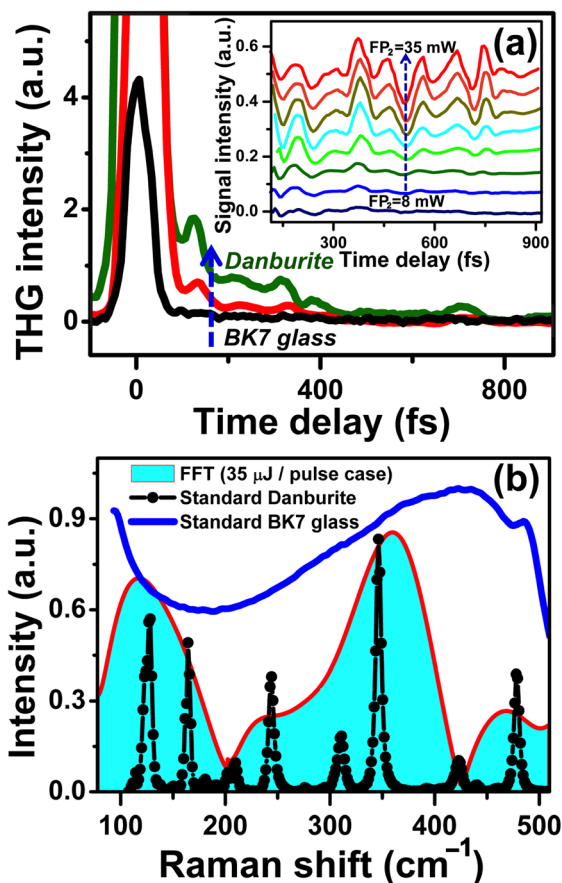


FIG. 4. (a) Laser irradiation power dependence of the quantum beats in BK7 glass. The inset shows stronger coherent oscillations with the increase of FP₂ power. (b) FFT spectrum of crystallized BK7 glass with the irradiation fs pulse energy of FP₂ at 35 μJ (red), in comparison with the standard Raman spectrum of BK7 glass (blue) and danburite crystal (black).

without any temporal oscillations [bottom curve, Fig. 4(a)], representing an autocorrelation signal of the incident FP pulse.¹² Since glass is long-range disordered, the THG signal generated at low power does not contain any significant CP modes due to poor band structure in the amorphous material where the phonons are strongly dispersed or scattered.¹⁴ As the FP₂ power is increased, THG temporal oscillations after ~ 100 fs are clearly observed and get further enhanced with higher power. The decay dynamics can be fitted with a single exponential with a time constant of ~ 350 fs, suggesting the involvement of some electronic population change upon intense photoexcitation.¹³ After subtracting the broad incoherent fit, the residual coherent oscillatory components at various FP₂ powers are shown in Fig. 4(a) inset. These dynamic traces directly reflect an increasingly ordered structure after fs laser irradiation on glass, where the CP modes experience longer mean free path leading to enhanced heat conductivity.^{14,29}

To identify the impulsively excited CP modes in crystallized BK7 glass, we use FFT to retrieve the underlying low-frequency modes responsible for TH₊₁ temporal oscillations with FP₂ of 35 $\mu\text{J}/\text{pulse}$ [Fig. 4(b)]. The standard Raman spectrum of BK7 glass shows a broad dominant $\sim 400\text{ cm}^{-1}$ band attributed to the Si–O–Si bond rocking and bending in the disordered matrix. The narrow 500 cm^{-1} peak is mainly assigned to the relatively smaller fourfold Si–O rings in the largely random silica network.⁵ However, the FFT spectrum of crystallized BK7 glass shows multiple characteristic peaks within $100\text{--}500\text{ cm}^{-1}$, significantly differing from amorphous glass or quartz (not shown). Previous experimental and theoretical studies proposed the formation of danburite-like structure units (e.g., including two SiO₄ and two BO₄ tetrahedra) in borosilicate glasses at high temperature and pressure.³⁰ The danburite Raman modes in the $100\text{--}500\text{ cm}^{-1}$ range are mainly attributed to stretching and bending modes of Si–O–Si groups as well as translational and rotational modes of the SiO₄ and BO₄ units.^{30,31} Eminently, the FFT spectrum of BK7 glass after fs laser irradiation shows good agreement in the peak positions and relative mode intensities with the danburite standard. The broad peak width in FFT could arise from incomplete and/or inhomogeneous crystallization³ as well as ephemeral CP dynamics that limits mode detection in the time domain.^{6,9} This key observation reveals that danburite-like structure units are forming at the glass surface after intense laser irradiation.

Using the aforementioned wavelet analysis, we further unravel the time evolution of each frequency-resolved CP mode embedded in the TH₊₁ signal trace with different FP₂ power [Figs. 5(a)–5(f)]. The usage of higher FP₂ power ensures that a local temperature increase is achieved for the measured CP dynamics on the sub-ps timescale because the microscale heat transfer typically occurs on the ps to μs timescale.³² With the FP₂ power increase, the dephasing time of each mode lengthens, suggesting the growth of microcrystalline structure at or near the laser focal point. Furthermore, incident-power-dependent frequency shifts of two marker modes are clearly observed. As shown in Fig. 5(g), the 150 cm^{-1} mode [FP₂ = 10 $\mu\text{J}/\text{pulse}$, see Fig. 5(a)] displays a monotonic redshift to $\sim 120\text{ cm}^{-1}$ with the increase of FP₂ power [Figs. 5(b)–5(f)], which indicates that laser-irradiated

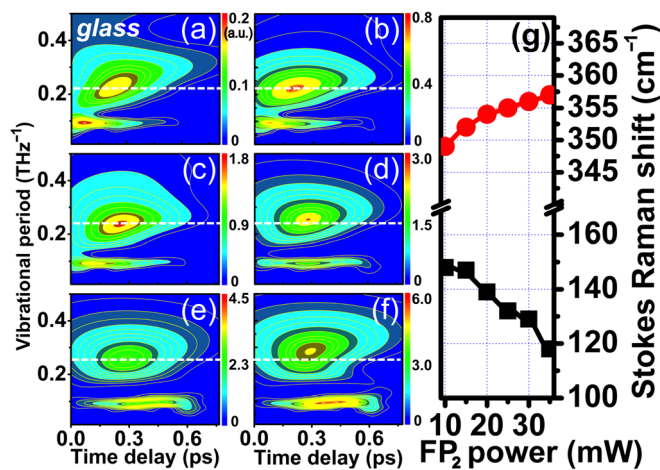


FIG. 5. Morlet wavelet-transformed time-frequency contour plot of the TH_{+1} temporal oscillations in BK7 glass at different FP_2 pulse energy of (a) $10 \mu\text{J}$, (b) $15 \mu\text{J}$, (c) $20 \mu\text{J}$, (d) $25 \mu\text{J}$, (e) $30 \mu\text{J}$, and (f) $35 \mu\text{J}$. The dashed lines evince a continuous redshift of the $\sim 150 \text{ cm}^{-1}$ mode with increasing FP_2 power, while the colorbars show that the wavelet-transform contour height increases in accord with stronger temporal oscillations of the THG signal. (g) The FP_2 -power dependent frequency shifts of two CP modes in crystallized BK7 glass.

phase changes occurring in the danburite-like crystal are due to temperature-induced thermal expansion.³³ Meanwhile, the 350 cm^{-1} mode manifests an opposite frequency change: a slight blueshift of $\sim 8 \text{ cm}^{-1}$. This anomalous behavior was observed in quartz crystal with a temperature increase from 300 to 900 K.³³ We thus surmise that the observed blueshift is due to an unusual thermal expansion of the B–O bond in the nascent danburite-like structure.³⁴

Can we substantiate the laser crystallization at glass surface without vibrational spectral analysis? Since a circularly polarized laser beam cannot generate THG in isotropic materials,³⁵ the order to disorder structure transformation in semiconductors could be tracked by the THG generated with a circularly polarized laser pulse.³⁶ In our previous report, we demonstrated that the THG signals in BK7 glass could be switched off as the two incident FP polarizations become perpendicular to each other.¹² Based on this recent finding, we hereby design a control experiment by adding a half waveplate into FP_1 beam to rotate its polarization state from p to s . The weak TH_{+1} signal intensity is measured via a lock-in amplifier with both FPs at $6 \mu\text{J}/\text{pulse}$. The laser crystallization is induced as the p -polarized FP_2 power is increased to $20 \mu\text{J}/\text{pulse}$ for ~ 6 min, followed by its power decrease to the original $6 \mu\text{J}/\text{pulse}$ for THG measurement. We observe a conspicuous $\sim 50\%$ increase of the TH_{+1} signal intensity, which clearly demonstrates that (1) the perpendicularly polarized FPs achieve optical switch and (2) crystalline thus anisotropic structure is formed at the BK7 glass surface by laser irradiation. More work on this tracking of material disorder to order phase changes will be reported in a future publication.

In conclusion, fs pulsed-laser-induced structural transformation of amorphous borosilicate glass is investigated using our recently developed TRSTHG spectroscopy. Results from polycrystalline CaF_2 clearly resolve the dominant coherent low-frequency Raman modes of the material by analyzing the highly sensitive, ubiquitous, and background-free THG signal generated in between the two incident FPs. Whereas in

amorphous BK7 glass, time-resolved quantum beats occur as the laser irradiation power reaches above $\sim 10 \mu\text{J}/\text{pulse}$. FFT analysis of the temporal oscillations elucidates characteristic CP modes indicative of a danburite-like crystalline structure, which is formed at the glass surface after several minutes of intense laser irradiation. In response to the increasing incident laser power, two marker CP modes display distinct frequency shifts. The atomic-level interplay between light (i.e., photons) and the electrical and vibrational forces (e.g., phonons) determines the conformation and dynamics of the atoms in the condensed phase, offering fundamental physical insights. More quantitative description can be obtained with theoretical modeling and calculations that are currently underway. Our technique represents a viable means to study directly in the time domain the collective nuclear motions accompanying electronic responses to determine the thermal and electrical conductivities of materials for myriad applications.

This research was supported by the Oregon State University Faculty Startup Research Grant and the College of Science Venture Fund Award to C.F.

- ¹N. H. Nickel, *Laser Crystallization of Silicon—Fundamentals to Devices* (Academic Press, Waltham, Massachusetts, 2003).
- ²J.-M. Shieh, Z.-H. Chen, B.-T. Dai, Y.-C. Wang, A. Zaitsev, and C.-L. Pan, *Appl. Phys. Lett.* **85**, 1232 (2004).
- ³B. Yu, B. Chen, B. Lu, X. Yan, J. Qiu, C. Zhu, and X. Jiang, *Crystr. Growth Des.* **7**, 30 (2007).
- ⁴X. C. Wang, H. Y. Zheng, C. W. Tan, F. Wang, H. Y. Yu, and K. L. Pey, *Opt. Express* **18**, 19379 (2010).
- ⁵F. L. Galeener, A. J. Leadbetter, and M. W. Stringfellow, *Phys. Rev. B* **27**, 1052 (1983).
- ⁶S. De Silvestri, J. G. Fujimoto, E. P. Ippen, E. B. Gamble, Jr., L. R. Williams, and K. A. Nelson, *Chem. Phys. Lett.* **116**, 146 (1985).
- ⁷P. Kukura, R. Frontiera, and R. A. Mathies, *Phys. Rev. Lett.* **96**, 238303 (2006).
- ⁸G. C. Cho, W. Kutt, and H. Kurz, *Phys. Rev. Lett.* **65**, 764 (1990).
- ⁹Y. M. Chang, L. Xu, and H. W. K. Tom, *Phys. Rev. Lett.* **78**, 4649 (1997).
- ¹⁰Y. R. Shen, *J. Opt. Soc. Am. B* **28**, A56 (2011).
- ¹¹D. Kupka, J. W. Wilson, O. Masihzadeh, and R. A. Bartels, *Chem. Phys. Lett.* **490**, 97 (2010).
- ¹²W. Liu, L. Wang, F. Han, and C. Fang, *Opt. Lett.* **38**, 3304 (2013).
- ¹³R. Merlin, *Solid State Commun.* **102**, 207 (1997).
- ¹⁴M. Born and K. Huang, *Dynamical Theory of Crystal Lattices* (Oxford University Press, New York, USA, 1998).
- ¹⁵Y. Wang, W. Liu, L. Tang, B. G. Oscar, F. Han, and C. Fang, *J. Phys. Chem. A* **117**, 6024 (2013).
- ¹⁶F. Han, W. Liu, and C. Fang, *Chem. Phys.* **422**, 204 (2013).
- ¹⁷L. Zhu, W. Liu, and C. Fang, *Appl. Phys. Lett.* **103**, 061110 (2013).
- ¹⁸A.-C. Tien, S. Backus, H. Kapteyn, M. Murnane, and G. Mourou, *Phys. Rev. Lett.* **82**, 3883 (1999).
- ¹⁹W. K. Burns and N. Bloembergen, *Phys. Rev. B* **4**, 3437 (1971).
- ²⁰J. P. Russell, *Proc. Phys. Soc.* **85**, 194 (1965).
- ²¹C. Chatfield, *The Analysis of Time Series: An Introduction*, 6th ed. (Chapman & Hall/CRC, Boca Raton, FL, 2004).
- ²²C. Wurster, K. Lassmann, and W. Eisenmenger, *Phys. Rev. Lett.* **70**, 3451 (1993).
- ²³S. N. Taraskin, Y. L. Loh, G. Natarajan, and S. R. Elliott, *Phys. Rev. Lett.* **86**, 1255 (2001).
- ²⁴T. S. Grigera, V. Martin-Mayor, G. Parisi, and P. Verrocchio, *Nature* **422**, 289 (2003).
- ²⁵J. W. Chan, T. Huser, S. Risbud, and D. M. Krol, *Opt. Lett.* **26**, 1726 (2001).
- ²⁶B. Yu, B. Chen, X. Yang, J. Qiu, X. Jiang, C. Zhu, and K. Hirao, *J. Opt. Soc. Am. B* **21**, 83 (2004).
- ²⁷E. N. Glezer, M. Milosavljevic, L. Huang, R. J. Finlay, T. H. Her, J. P. Callan, and E. Mazur, *Opt. Lett.* **21**, 2023 (1996).
- ²⁸Y. Li, W. Watanabe, K. Yamada, T. Shinagawa, K. Itoh, J. Nishii, and Y. Jiang, *Appl. Phys. Lett.* **80**, 1508 (2002).
- ²⁹A. J. Minnich, J. A. Johnson, A. J. Schmidt, K. Esfarjani, M. S. Dresselhaus, K. A. Nelson, and G. Chen, *Phys. Rev. Lett.* **107**, 095901 (2011).

- ³⁰D. Manara, A. Grandjean, and D. R. Neuville, *J. Non-Cryst. Solids* **355**, 2528 (2009).
- ³¹S. P. Best, R. J. H. Clark, C. L. Hayward, and R. Withnall, *J. Raman Spectrosc.* **25**, 557 (1994).
- ³²S. Link and M. A. El-Sayed, *Int. Rev. Phys. Chem.* **19**, 409 (2000).
- ³³P. Gillet, A. Le Cléac'h, and M. Madon, *J. Geophys. Res., [Solid Earth]* **95**, 21635, doi:10.1029/JB095iB13p21635 (1990).
- ³⁴K. Sugiyama and Y. Takéuchi, *Z. Kristallogr.* **173**, 293 (1985).
- ³⁵T. Tsang, *Phys. Rev. A* **54**, 5454 (1996).
- ³⁶V. V. Yakovlev and S. V. Govorkov, *Appl. Phys. Lett.* **79**, 4136 (2001).